

Enhanced Electrochemical Performance of $0.4\text{Li}_2\text{MnO}_3\text{-}0.6\text{LiMn}_{0.35}\text{Ni}_{0.3}\text{Co}_{0.35-x}\text{Al}_x\text{O}_2$

Dongyun Zhang^{1,*}, Wenping Li¹, Nan Li¹, Jin Qiao¹, Zifeng Ma² and Chengkang Chang^{1,3,*}

¹ School of Materials Science and Engineering, Shanghai Institute of Technology, 100 Haiquan Road, Shanghai 201418, China

² School of Chemistry and Chemical Engineering, Shanghai Jiaotong University, 800 Dongchuan Road, Shanghai 200240, China

³ Shanghai Institute of Innovative Materials, Shanghai University, 99 Shangda Road, Shanghai, 200444, China

*E-mail: dyz@sit.edu.cn

Received: 4 March 2018 / Accepted: 9 May 2018 / Published: 5 June 2018

$0.4\text{Li}_2\text{MnO}_3\text{-}0.6\text{LiMn}_{0.35}\text{Ni}_{0.3}\text{Co}_{0.35-x}\text{Al}_x\text{O}_2$ layered structured cathode materials have been successfully prepared via a high temperature solid state method with different Al contents. X-Ray diffraction (XRD), scanning electron microscopy (SEM), cyclic tests, electrical conductivity tests and electrochemical impedance spectrum (EIS) were employed to investigate the reason for the enhanced electrochemical performances. XRD and SEM results revealed that the introduction of Al into the lattice determines the interlayer spacing and thus the growth manner of the crystals and greatly promotes the electrochemical performance. At $x=0.05$, the maximum values achieved are 249.9 mAh/g for the initial specific capacity and 99.2% for the capacity retention after 50 cycles. Such good results are caused by the improvement in both the electrical conductivity and the Li ion conductivity. The electrical conductivity for the pristine material without Al doping is measured as $2.52 \times 10^{-8} \text{ S cm}^{-1}$, while the sample with $x=0.05$ exhibits a value of $8.87 \times 10^{-8} \text{ S cm}^{-1}$. The calculated Li ion diffusion also shows similar results, confirming the promotion of the electrochemical performances after Al incorporation into the layered structure. All the results demonstrate that Al doped layered material is very promising for use as a cathode for lithium secondary batteries.

Keywords: lithium ion battery, electrical conductivity, specific capacity, impedance, cyclic performance

1. INTRODUCTION

Lithium-rich manganese-based materials have been widely studied in the past decade for their enormous potential to serve as cathode electrodes for next generation Li ion batteries due to their theoretical specific capacity of over 300 mAh/g[1, 2]. Their crystal structure has also been studied, and

the results confirmed that such materials are regarded as a solid solution of two different layered structure components, such as the Li_2MnO_3 and LiMO_2 phases (where $M = \text{Co}, \text{Ni}, \text{Mn}$) [3]. Therefore, various compositions with different combinations of Li_2MnO_3 and LiMO_2 (such as $x \text{Li}_2\text{MnO}_3 (1-x) \text{LiMO}_2$) have been studied for actual applications in LIBs in recent years [4, 5]. The component Li_2MnO_3 is thought to be electrochemically inactive because of the presence of Mn in its +4 oxidation state. However, when this material was charged above 4.5 V, electrochemical behaviors were observed in it due to the structure of the MnO_2 , which can be employed to reversibly intercalate lithium ions [6]. It was also found by these studies that the use of cobalt and nickel components in the layered structures helps in reducing the electrode polarization and leads to stable electrochemical performance [7].

One of the defects of the materials is their low capacity retention, which has been the focus of study for many scholars [8, 9]. Several mechanisms have been proposed to explain the first cycle behavior in these electrode systems using different methods. Armstrong [10], in their recent paper, suggested that the flat charge profile can be explained by the oxygen loss from the surface and the diffusion of the transition metal ions from the outside to inside of the bulk. Tran [11] suggested a model of the migration of oxygen from the inside to the outside of the bulk for the first cycle behavior, and they also agreed that the plateau is associated with the migration of the transition metal ions. Recent studies in this field have considered the simultaneous removal of oxygen and lithium during the first cycle, followed by cation migration from transition metal layers to lithium layers [12].

The above works were valuable. Further works based on these pioneering studies provided applicable samples with high specific capacity and stable cycling performance [13-14]. Due to the selective use of M ions, many systems have been developed, and new approaches have been employed to determine an optimal manufacturing process. Among these methods, the sol-gel, hydrothermal, coprecipitation and spray pyrolysis methods were attempted [15-19]. Recent works have also focused on ion doping and surface coating approaches to increase the specific capacity and reduce capacity fading. Al atom doping was regarded as an effective way to prevent capacity fading when the atoms were incorporated into the lattice sites in certain $x\text{Li}_2\text{MnO}_3 - (1-x) \text{LiMO}_2$ systems [20-22].

In this paper, we proposed a new approach for the synthesis of layer structured Li-rich cathode materials. $0.4\text{Li}_2\text{MnO}_3 - 0.6\text{LiMn}_{0.35}\text{Ni}_{0.3}\text{Co}_{0.35}\text{O}_2$ was selected as the mother compound, and Al atoms supposedly doped the original Co lattice sites; therefore, the nominated compound can be designated $0.4\text{Li}_2\text{MnO}_3 - 0.6\text{LiMn}_{0.35}\text{Ni}_{0.3}\text{Co}_{0.35-x}\text{Al}_x\text{O}_2$. Samples with various x values were calcined at 850°C and the related electrochemical properties were evaluated. The electrochemical behaviors were greatly enhanced by Al doping, and optimal results were obtained at $x=0.05$ with an initial specific capacity of 249.9 mAh/g and a capacity retention of 99.2% after 50 runs. Such results indicate the high potential of the material for use as a cathode in LIBs.

2. EXPERIMENTAL

2.1. Synthesis of the cathode materials

The cathode materials $0.4\text{Li}_2\text{MnO}_3 - 0.6\text{LiMn}_{0.35}\text{Ni}_{0.3}\text{Co}_{0.35-x}\text{Al}_x\text{O}_2$ with different Al contents were synthesized by a solid-state process. Lithium hydroxide (99.5%), manganese oxide (99.5%),

nickel oxide, (99.5%), cobalt oxide (99.5%) and aluminum oxide (99.5%) were used as raw materials, which were mixed and ground using a ball miller for 4 h in water. Then, the obtained slurry was dried by a spray dryer, and spherical precursors were obtained. Finally, the precursors were calcined at 850°C for 12 h in an air atmosphere, and black cathode powders with different aluminum contents were obtained.

2.2. Characterization of the prepared powders

X-Ray diffraction (XRD) profiles were collected with a TD3200 X-ray diffractometer using Cu K α radiation. The data were collected from 10° to 70° (2 θ) using a continuous scanning mode. The morphologies of the prepared samples were monitored via scanning electron microscopy (SEM). The electrical conductivity (EC) of the synthesized materials was measured at room temperature using a powder resistivity tester FT-300/301, in which the powder was compressed into disc like samples with a diameter of 10 mm under pressure from 2 MPa to 22 MPa.

2.3. Electrochemical testing

The electrodes were fabricated by blending the active material (0.4Li₂MnO₃-0.6LiMn_{0.35}Ni_{0.3}Co_{0.35-x}Al_xO₂) with the acetylene black as a conductive additive and PVDF as a binder at a weight ratio of 8:1:1 in N-methyl-2-pyrrolidone (NMP). The mixture was first pasted onto an aluminum foil and then dried at 110 °C in a vacuum oven for 12 hours. The thickness of the coating materials was controlled to be approximately 0.030 mm. The dried samples were rolled into their final thickness of 0.015-0.025 mm. Next, electrodes were prepared by cutting the foils into discs with a diameter of 12 mm.

The electrochemical performances of the cathode materials were evaluated using coin cells. All the cells were assembled in a glove box filled with Ar. The cells were galvanostatically charged and discharged with a Land CT2001 battery tester at a voltage of 2.0-4.8 V for 50 runs. The specific capacities of the samples were calculated based on the weight of the synthesized materials in the cathode. Electrochemical impedance spectroscopy (EIS) was carried out using an electrochemical workstation (Autolab Pgstat302n) over a frequency range of 100 kHz-0.01 Hz under fully discharging condition using coin-type cells.

3. RESULTS AND DISCUSSION

3.1. Phase purity and determination of the structural influence of Al doping

XRD profiles of the cathode materials with different x values (x=0, 0.03, 0.05, 0.1, 0.15) are presented in Fig.1. It is clear from the patterns that all the samples prepared with different Al contents present a pure phase structure. All the peaks in the pattern can be indexed to the NaFeO₂-type layered structure with space group R3m, and the detailed indexes of the peaks are also marked on the figure.

Furthermore, separation between the adjacent peaks of (018)/(110) can be clearly observed, implying a typical layered structure of the prepared cathode materials. No additional peaks corresponding to Al containing phases can be observed, showing that the Al atoms have been introduced into the crystal lattice.

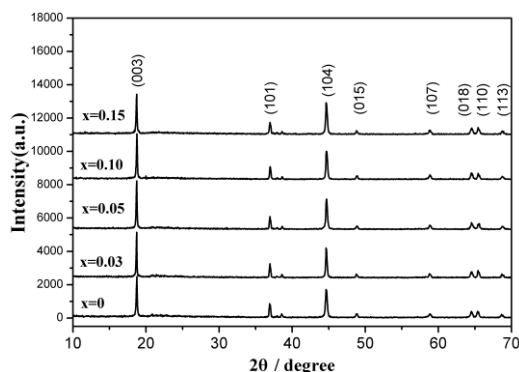


Figure 1. XRD profiles of the $0.4\text{Li}_2\text{MnO}_3\text{-}0.6\text{LiMn}_{0.35}\text{Ni}_{0.3}\text{Co}_{0.35-x}\text{Al}_x\text{O}_2$ samples with various x values

The refined lattice parameters for the different samples are listed in Table 1, together with the intensity ratio of $I(003)/I(104)$. The data show that when a small amount of Al atoms was introduced, no obvious change in the a axis could be observed, but a significant change in the c axis could be observed. It is found from the table that with the increase in the amount of Al introduced, the c axis increases gradually, reaches the maximum at $x=0.10$ and decreases with further increasing x value. Such changes in lattice parameters can be explained by the disturbance of the crystal environment due to the atomic doping of the pristine material by Al atoms. The most significant difference in the data listed in the table is observed for the intensity ratio of $I(003)/I(104)$ of the prepared samples. This ratio is commonly regarded as important for Li ion exchange between the cathode material and the electrolyte because its value reflects the interlayer spacing of the layered structure. The larger the ratio is, the better the electrochemical performances are. In our case, with the increase in the x value, the $I(003)/I(104)$ ratio reaches a maximum value at $x=0.05$, implying that the promotion of electrochemical performance could be achieved by the introduction of Al atoms into the crystal lattice, and therefore, better electrochemical properties are expected.

Table 1. Calculated lattice parameters and related ratio of $I(003)/I(104)$ for the $0.4\text{Li}_2\text{MnO}_3\text{-}0.6\text{LiMn}_{0.35}\text{Ni}_{0.3}\text{Co}_{0.35-x}\text{Al}_x\text{O}_2$ samples

x value	Lattice parameters			$I(003)/I(104)$
	$a(\text{\AA})$	$c(\text{\AA})$	$V(\text{\AA}^3)$	
0	2.856	14.143	99.86	1.321
0.03	2.856	14.162	100.04	1.345
0.05	2.858	14.197	100.31	1.598
0.10	2.857	14.213	100.47	1.406
0.15	2.858	14.176	100.21	1.268

3.2. Crystal shape changes with different Al contents

Fig. 2 shows typical SEM micrographs of the prepared samples. Fig. 2a presents the common features of the prepared powders, in which spherical particles were presented. An enlarged micrograph of an individual particle is illustrated in Fig. 2b, where porous microstructures were observed, due to the dehydration of the lithium hydroxide during the spray drying process employed in the experiment.

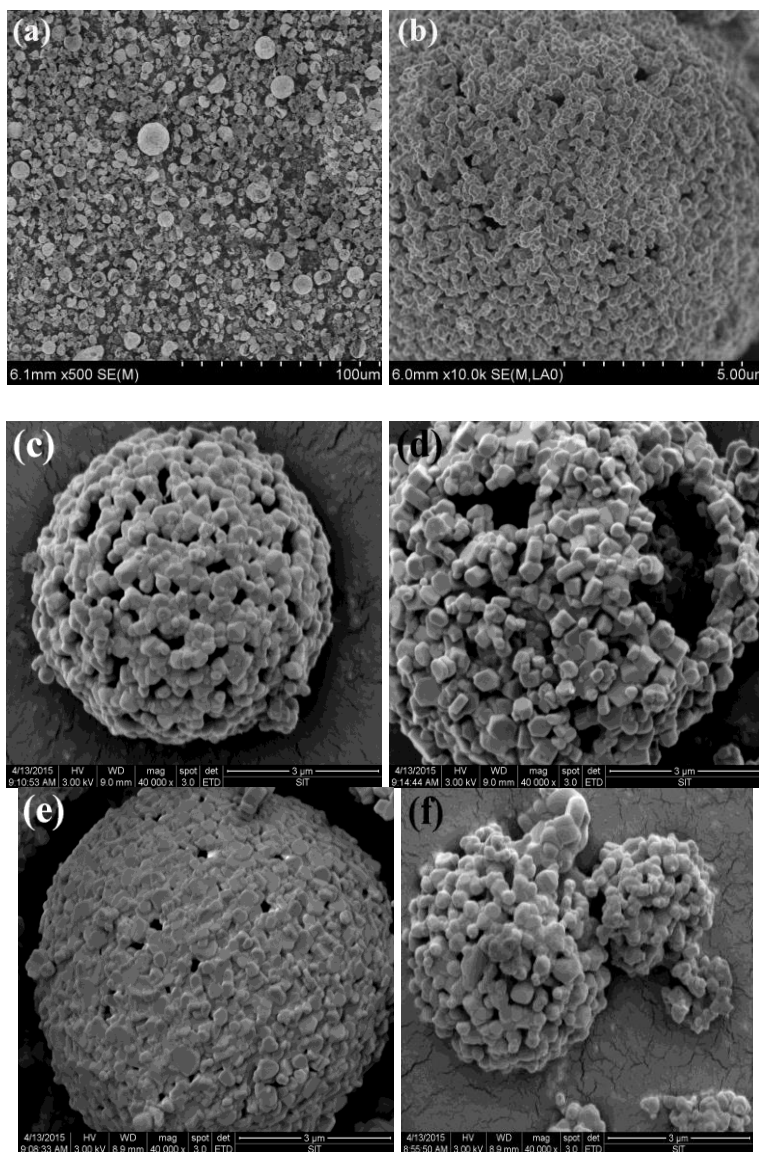


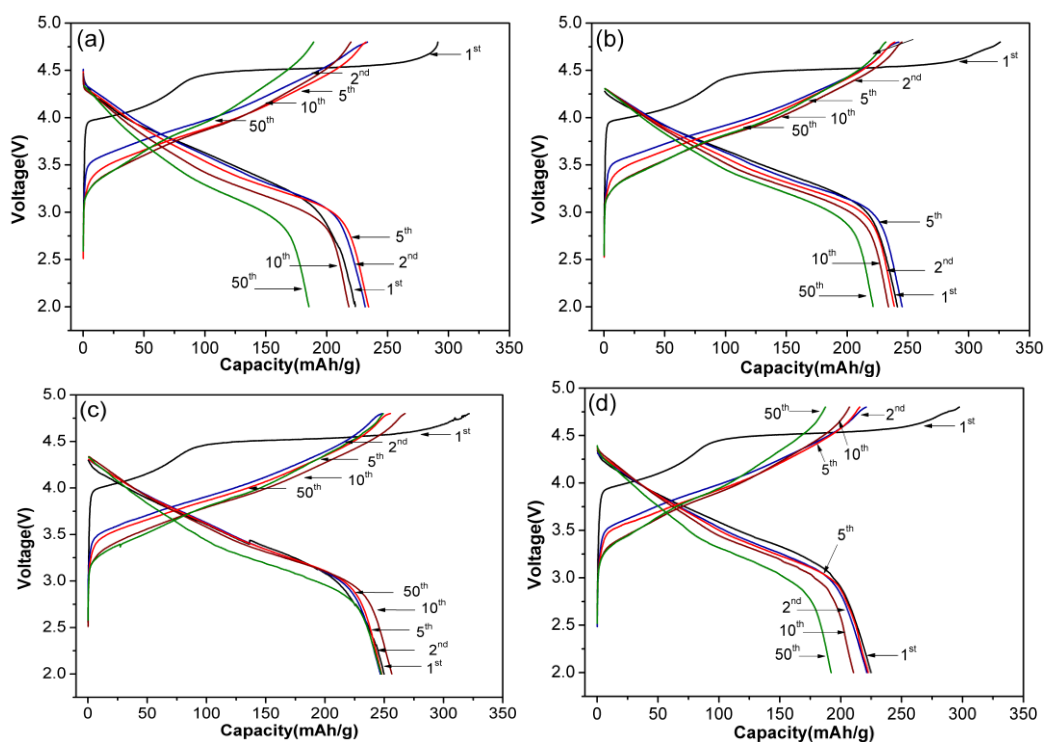
Figure 2. SEM micrographs of the $0.4\text{Li}_2\text{MnO}_3\text{-}0.6\text{LiMn}_{0.35}\text{Ni}_{0.3}\text{Co}_{0.35-x}\text{Al}_x\text{O}_2$ samples: (a) and (b), typical micrographs, and micrographs for sample with (c), $x=0$, (d), $x=0.03$, (e), $x=0.05$ and (f), $x=0.10$

However, morphological differences were also observed by comparing the SEM micrographs of samples prepared with different Al contents. Fig. 2c - Fig. 2f show the differences with x values from 0-10%. It can be seen from Fig. 2c that round-like crystals without obvious shapes were

generated at $x=0$. However, at $x=0.03$, crystals with columnar shapes were created, as confirmed in Fig. 2d. At $x=0.05$, platy crystals were clearly observed, suggesting that good layered structures were obtained. Further increases in the x values, however, did not show positive results, and round-like crystals were observed again. Such differences in the crystal shape suggest that the growth manner of the layered structures is greatly influenced by the amount of Al introduced. The reason is not yet clear and will be discussed elsewhere. It should be noted here that the changes in crystal shape with the different Al contents are in good accordance with the XRD findings of the changes in the (003)/(104) ratios with the x values, which further implies that the introduction of Al into the lattice sites is an efficient method to control the growth manner and the interlayer spacing.

3.3. Enhancement of electrochemical performance by Al doping

The electrochemical performances of the synthesized cathodic samples were investigated by charge-discharge cyclic tests. Fig. 3 shows the cyclic curves of the sample powders with different Al contents cycled between 2.0 and 4.8 V at room temperature and at a constant current density of 50 mA/g. All the samples had similar charge and discharge curves. The initial charge curve of the composite powders could be divided into two main parts. One comes from the process of the removal of lithium from the $\text{LiMn}_{0.35}\text{Ni}_{0.3}\text{Co}_{0.35-x}\text{Al}_x\text{O}_2$ component, shown by the smoothly sloping voltage profile below 4.5 V. The other comes from the removal of Li_2O from the Li_2MnO_3 component, which could be confirmed by the clear voltage plateau above 4.5 V in the figures, as reported by other studies [23-25].



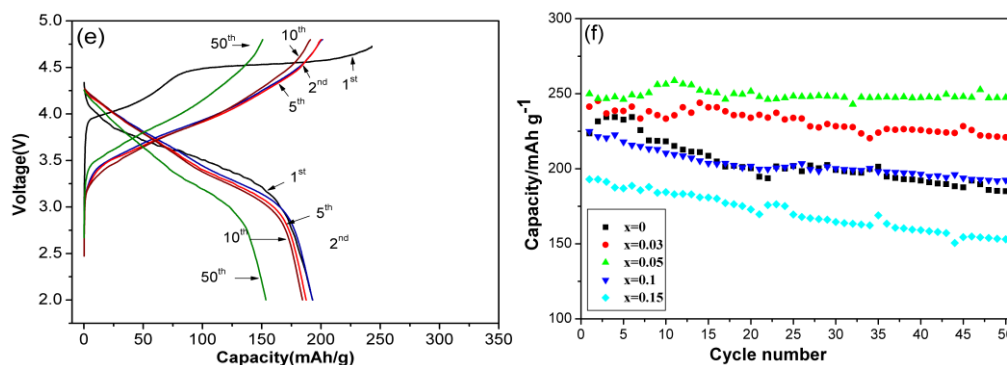


Figure 3. Cyclic performance of the $0.4\text{Li}_2\text{MnO}_3\text{-}0.6\text{LiMn}_{0.35}\text{Ni}_{0.3}\text{Co}_{0.35-x}\text{Al}_x\text{O}_2$ samples at a constant current density of 50 mA/g for 50 cycles (a), $x=0$, (b), $x=0.03$, (c), $x=0.05$, (d), $x=0.10$, (e), $x=0.15$, and (f), comparison between the 5 samples.

For the cathode materials, the initial specific capacity and the capacity retention are the key factors that determine the actual performance in the battery industry. Fig. 3a shows the cyclic behaviors of the pristine $0.4\text{Li}_2\text{MnO}_3\text{-}0.6\text{LiMn}_{0.35}\text{Ni}_{0.3}\text{Co}_{0.35}\text{O}_2$ without Al addition. The initial capacity in the first run is 234.3 mAh/g, and the fading in specific capacity is very fast; only 79.1% capacity retention was observed after 50 runs. These results are very similar to the values reported in other studies. However, by introducing Al atoms into the lattice sites, electrochemical behaviors were promoted. With the increase in Al content, the initial specific capacity increases up to 249.9 mAh/g at $x=0.05$ and then gradually decreases to 193.2 mAh/g at $x=0.15$, as shown in Fig. 3b to Fig. 3e. The detailed data at different x values are listed in Table 2. It can be seen from the table that the change in capacity retention shows similar results. It reaches 99.2% with $x=0.05$ and then decreases to 79.3% with $x=0.15$. The above results greatly imply that the incorporation of Al atoms into the crystal sites has great effects on the electrochemical performance of the prepared cathode materials.

Table 2. Specific capacities and capacity retentions in different runs with different x values

x values	1 st	2 nd	5 th	10 th	50 th	Capacity retention
0	234.3	232.1	224.1	217.5	185.4	79.1%
0.03	241.4	245.3	238.5	233.4	221.3	91.7%
0.05	249.9	246.7	246.2	256.4	247.5	99.2%
0.1	224.9	221.4	217.9	210.5	192.4	85.7%
0.15	193.2	192.9	186.9	184.4	153.2	79.3%

A comparison of the discharge capacity and cycle retention rate of lithium-rich manganese-based materials with doping of various metal ions reported by other scholars [26-29] and this work is shown in Table 3. The discharge specific capacity and cycle retention rate of the $0.4\text{Li}_2\text{MnO}_3\text{-}0.6\text{LiMn}_{0.35}\text{Ni}_{0.3}\text{Co}_{0.3}\text{Al}_{0.05}\text{O}_2$ prepared in this work are better than most of the reported results [27-29], except for the Ca^{2+} doped lithium-rich manganese-based materials [26], as shown in Table 3. Iftekhar [29] also worked on Al doping of lithium-rich manganese-based materials. According to their work,

the discharge specific capacity of $\text{Li}_{1.16}\text{Ni}_{0.167}\text{Mn}_{0.49}\text{Al}_{0.01}\text{Co}_{0.167}\text{O}_2$ was 201 mAh/g at a current density of 15 mA/g, which is much lower than the values obtained in this work. $\text{Li}_{1.2}\text{Ni}_{0.13}\text{Co}_{0.13}\text{Mn}_{0.44}\text{Co}_{0.1}\text{O}_2$ [28] had a comparable discharge specific capacity of 248 mAh/g, which was obtained at a lower current density (25 mA/g), but its capacity retention was only 88.8% after 50 cycles.

Table 3. Comparison of the electrochemical properties of lithium-rich manganese-based materials obtained from references [26-29] and this work.

Doped ions	Doping amount	Discharge specific capacity(mAh/g)	Rates(mA/g)	Capacity retention	Cycle number
Al^{3+}	0	243.3	50	79.1%	50
	0.03	241.4		91.7%	
	0.05	249.9		99.2%	
	0.1	224.9		85.7%	
	0.15	193.2		79.3%	
Ca^{2+} [26]	0.002	246	50	82%	100
	0.005	273		87%	
	0.007	256		85%	
	0.01	233		81%	
	0.03	218		74%	
Mg^{2+} [27]	0.024	195.4	50	-	-
	0.048	177.7		-	-
	0.072	162.3		-	-
Co^{3+} [28]	0.05	245	25	87.8%	50
	0.10	248		88.8%	
	0.15	240		62%	
Cr^{3+} [28]	0.05	230	25	82.6%	50
	0.10	224		93.7%	
	0.15	240		90.4%	
Fe^{3+} [28]	0.05	230	25	90.4%	50
	0.10	208		72.1%	
	0.15	174		58.6%	
Al^{3+} [29]	0.01	201	15	88%	100
	0.02	180		91%	

3.4. Improvement of electrical conductivity by Al doping

To reveal the importance of Al in the electrochemical process, the changes in the electrical conductivity and the changes in the Li ion diffusion coefficient before and after Al atom doping are very important and should be taken into account. The electrical conductivities of the prepared cathode materials were measured and are shown in Fig. 4. When calculated from the figure, the electrical conductivity of the pristine material is confirmed as $2.52 \times 10^{-8} \text{ S cm}^{-1}$, while the value for the sample with $x=0.05$ is approximately $8.87 \times 10^{-8} \text{ S cm}^{-1}$, several times the value of the pristine sample. The promotion of electrical conductivity is obvious. It can be seen from the figure that with the increase in Al content, the electrical conductivity reaches its maximum value of at $x=0.05$ and then sharply

decreases. The result indicates that Al doping can effectively improve the conductivity of the cathode materials at a certain amount.

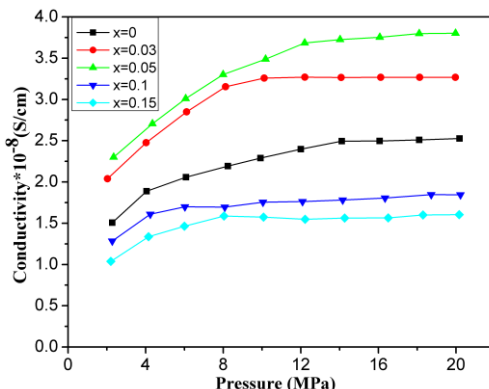


Figure 4. The electrical conductivity of the $0.4\text{Li}_2\text{MnO}_3\text{-}0.6\text{LiMn}_{0.35}\text{Ni}_{0.3}\text{Co}_{0.35-x}\text{Al}_x\text{O}_2$ samples.

3.5. Enhancement of Li diffusion by Al doping

To further reveal the reason for the enhancement of properties by Al doping, EIS testing was conducted to calculate the Li ion diffusion coefficients. Fig. 5a demonstrates the Nyquist plots of $0.4\text{Li}_2\text{MnO}_3\text{-}0.6\text{LiMn}_{0.35}\text{Ni}_{0.3}\text{Co}_{0.35-x}\text{Al}_x\text{O}_2$ in the fully discharged state. The intercept on the Z' axis in the high frequency region relates to the ionic conductivity of the electrolyte. The semicircles in the high-to-medium frequency range are associated with the charge transfer between the electrolyte and the cathode material. At very low frequencies (0.01Hz-1Hz in our case), the typical Warburg behavior can be attributed to the solid-state diffusion of lithium ions.

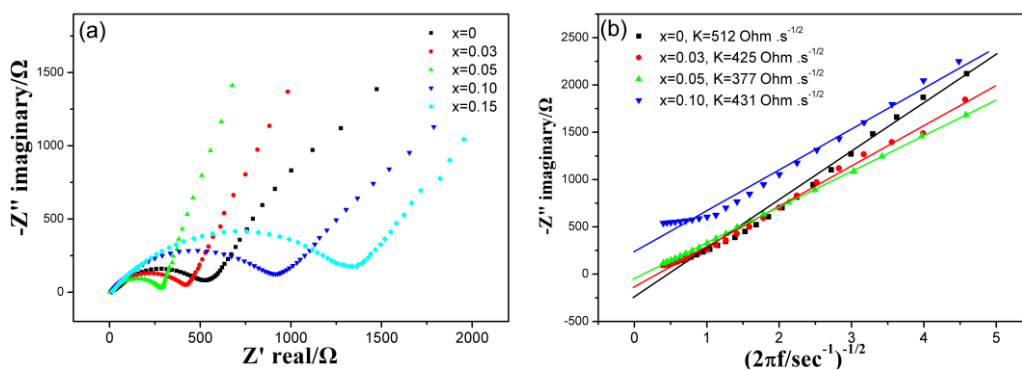


Figure 5. EIS results of the prepared samples over a frequency range of 100 kHz-0.01 Hz under the fully discharged condition. (a), Nyquist plot of the EIS of coin cells, and (b), the linear relationship between the Warburg impedance and the inverse square root of the angular frequency; the slopes of the simulated lines are the Warburg constant for the samples.

According to the model proposed by Ho [30], the diffusion coefficient of Li ions can be calculated using Eq. (1):

$$D_{Li} = 1/2[(V_M / SFA)(\delta E / \delta x)]^2 \quad (1)$$

where V_M is the molar volume ($38.08 \text{ cm}^3/\text{mol}$ in our case), S is the contact area between the electrolyte and sample (1.13 cm^2), F is the Faraday constant (96486 C/mol), and $\delta E / \delta x$ is the slope of the coulometric titration curve obtained from the cyclic curves. The constant A can be obtained from the Warburg impedance according to the following equation:

$$W = A\omega^{-1/2} \quad (2)$$

ω is the angular frequency, and can be express as a function of the frequency employed in the test by the following equation:

$$\omega = 2\pi f \quad (3)$$

Fig. 5b shows the linear fitting of Z' vs. $\omega^{1/2}$ at low frequency in the frequency values range from 0.01 Hz to 1 Hz, with different slopes varying from 512 to 431 $\text{Ohm s}^{-1/2}$. Therefore, the diffusion coefficients of Li ions were calculated as listed in Table 4.

Table 4. D_{Li} of $0.4\text{Li}_2\text{MnO}_3\text{-}0.6\text{LiMn}_{0.35}\text{Ni}_{0.3}\text{Co}_{0.35-x}\text{Al}_x\text{O}_2$ calculated from EIS results

	X=0	X=0.03	X=0.05	X=0.10
A(Ohm s ^{-1/2})	512	425	377	431
$\delta E / \delta x$ (V/mol)	1.34	1.47	1.69	1.38
D_{Li} (cm ² /s)	4.18×10^{-13}	7.29×10^{-13}	1.22×10^{-12}	6.25×10^{-13}

The D_{Li} obtained in our case is relatively low compared to other cathode materials, showing the difficulty for Li ions to migrate among the crystal lattice. To confirm the correctness of the calculation, document searching of such data was carried out. We found that our result agrees well with the data reported by X. Jin [31]. For the sample without Al doping, the diffusion coefficient is $4.18 \times 10^{-13} \text{ cm}^2/\text{s}$. After Al incorporation, the diffusion is greatly improved, and the value reaches a maximum of $1.22 \times 10^{-12} \text{ cm}^2/\text{s}$, several times the value of the pristine material. Therefore, it can be concluded that, a suitable amount of Al incorporated into the crystal is helpful for the migration of Li ions within the crystal structure and thus improves the electrochemical behaviors.

4. CONCLUSION

In summary, $0.4\text{Li}_2\text{MnO}_3\text{-}0.6\text{LiMn}_{0.35}\text{Ni}_{0.3}\text{Co}_{0.35-x}\text{Al}_x\text{O}_2$ layered structured cathode materials have been successfully prepared via a high temperature solid-state method with different Al contents. The influences of Al doping on the crystal structure, crystal growth manner and related electrochemical behaviors were investigated. At $x=0.05$, the prepared sample has the largest $I(003)/I(104)$ value, which leads to a great promotion in both the initial capacity and the capacity retention after 50 runs. The maximum values achieved in the experiment are 249.9 mAh/g for the initial specific capacity and 99.2% for the capacity retention after 50 cycles. Such good results are caused by the promotion in both the electrical conductivity and the Li ion conductivity. The electrical conductivity for the pristine material without Al doping is measured as $2.52 \times 10^{-8} \text{ S cm}^{-1}$, while the sample with $x=0.05$ exhibits a value of $8.87 \times 10^{-8} \text{ S cm}^{-1}$. The calculated Li ion diffusion also shows similar results, confirming the promotion of the electrochemical performances after Al incorporation

into the layered structure. All the results demonstrate that Al-doped layered material is very promising for use as a cathode in lithium secondary batteries.

ACKNOWLEDGEMENTS

We gratefully acknowledge the financial support by the Innovation Program of Shanghai Municipal education commission (15ZZ095) and the Science and Technology Commission of Shanghai Municipality (14520503100).

References

1. Z. Lu, L.Y. Beaulieu, R. A. Donaberger, C. L. Thomas and J. R. Dahn, *J. Electrochem. Soc.*, 149 (2002) A778.
2. M. M. Thackeray, S. H. Kang, C. S. Johnson, J. T. Vaughey, R. Benedek and S. A. Hackney, *J. Mater. Chem.*, 17 (2007) 3112.
3. C. S. Johnson, J. S. Kim, C. Lefief, N. Li, J. T. Vaughey and M. M. Thackeray, *Electrochem. Commun.*, 6 (2004) 1085.
4. Y. Wu and A. Manthiram, *Solid State Ionics*, 180 (2009) 50.
5. T. A. Arunkumar and Y. Wu, A. Manthiram, *Chem. Mater.*, 19 (2007) 3067.
6. C. H. Lei, J. Baren, J. G. Wen, I. Petrov, S. H. Kang and D. P. Abraham, *J. Power Sources*, 178 (2008) 422.
7. S. H. Kang, P. Kempgens, S. Greenbaum, A. J. Kropf, K. Amine and M. M. Thackeray, *J. Mater. Chem.*, 17 (2007) 2069.
8. N. Li, Y.S. He and X.P. Wang, *Electrochim. Acta*, 231 (2017) 363.
9. Z. Q. Deng and A. Manthiram, *J. Phys. Chem. C*, 115 (2011) 7097.
10. R. Armstrong, M. Holzapfel, P. Novák, C. S. Johnson, S. H. Kang, M. M. Thackeray. and P. G. Bruce, *J. Am. Chem. Soc.*, 128 (2006) 8694.
11. N. Tran, L. Croguennex, M. Menetrier, F. Weill, P. Biensan, C. Jordy and C. Delmas, *Chem. Mater.*, 20 (2008) 4815.
12. A. Ito, K. Shoda, Y. Sato, M. Hatano, H. Horie and Y. Ohsawa, *J. Power Sources*, 196 (2011) 4785.
13. Y. L. Wang, X. Huang, F. Li, J. S. Cao and S. H. Ye, *RSC Adv.*, 5 (2015) 49651
14. E. Zhao, Z. Hu, L. Xie, X. Chen, X. Xiao and X. Liu, *RSC Adv.*, 5 (2015) 31238
15. Y. S. Jang, J. H. Kim, J.K. Lee, B. K. Park and Y. C. Kang, *Int. J. Electrochem. Sci.*, 7 (2012) 12370.
16. A. Choi, K. Palanisamy, Y. Kim, J. Yoon, J. H. Park, S. W. Lee, W. Yoon and K. Kim, *J. Alloy. Compd.*, 591 (2014) 356.
17. X. Miao, Y. Yan, C. Wang, L. Cui, J. Fang and G. Yang, *J. Power Sources*, 2014, 247, 219-227
18. S. Shi, S. Zhang, Z. Wu, T. Wang, J. Zong, M. Zhao and G. Yang, *J. Power Sources*, 337 (2017) 82.
19. J. Shojan, C. V. Rao, L. Torres, G. Singh and R. S. Katiyar, *Mater. Lett.*, 104 (2013) 57.
20. E. Lee, R. Koritala, D. J. Miller, and C. S. Johnson, *J. Electrochem. Soc.*, 162 (3) (2015) A322.
21. H. Konishi, A. Gunji, X. Feng and S. Furutsuki, *J. Solid State Chem.*, 2017, 249:80-86.
22. J. H. Kim and Y.C. Kang, *Int. J. Electrochem. Sci.*, 8 (2013) 3664.
23. S. Rajarathinam, S. Mitra and R. K. Petla, *Electrochim. Acta*, 108 (2013) 135.
24. Y. Xiang, Z. Yin, Y. Zhang and X. Li, *Electrochim. Acta*, 91 (2013) 214.
25. K. Karthikeyan S. Amaresh, S.H. Kim, V. Aravindan and Y.S. Lee, *Electrochim. Acta*, 108 (2013) 749.
26. C.P. Laisaa, R.N. Ramesha and K. Ramesh, *Electrochim. Acta*, 256 (2017) 10.

27. Y. Xiang, J. Li, X. Wu, Z. Liu, L. Xiong, Z. He and Z. Yin, *Ceram. Int.*, 42 (2016) 8833
28. R.N. Ramesha, C.P. Laisa and K. Ramesha, *Electrochim. Acta*, 249 (2017) 377.
29. M. Iftexhar, N. E. Drewett, A. R. Armstrong, D. Hesp, F. Braga, S. Ahmed, and L. J. Hardwick, *J. Electrochem. Soc.*, 161 (14) (2014) A2109.
30. C. Ho, I. D. Raistrick and R. A. Huggins, *J. Electrochem. Soc.*, 127 (1980) 343.
31. X. Jin, Q. Xu, H. Liu, X. Yuan and Y. Xia, *Electrochim. Acta*, 136 (2014) 19.

© 2018 The Authors. Published by ESG (www.electrochemsci.org). This article is an open access article distributed under the terms and conditions of the Creative Commons Attribution license (<http://creativecommons.org/licenses/by/4.0/>).